arXiv:2211.14646v1 [cs.CV] 26 Nov 2022

Towards Better Input Masking for Convolutional Neural Networks

Sriram Balasubramanian
University of Maryland, College Park
sriramb@umd.edu

Soheil Feizi
University of Maryland, College Park
sfeizi@umd.edu

Abstract

The ability to remove features from the input of machine learning models is very important to understand and interpret model predictions. However, this is non-trivial for vision models since masking out parts of the input image and replacing them with a baseline color like black or grey typically causes large distribution shifts. Masking may even make the model focus on the masking patterns for its prediction rather than the unmasked portions of the image. In recent work, it has been shown that vision transformers are less affected by such issues as one can simply drop the tokens corresponding to the masked image portions. They are thus more easily interpretable using techniques like LIME which rely on input perturbation. Using the same intuition, we devise a masking technique for CNNs called layer masking, which simulates running the CNN on only the unmasked input. We find that our method is (i) much less disruptive to the model's output and its intermediate activations, and (ii) much better than commonly used masking techniques for input perturbation based interpretability techniques like LIME. Thus, layer masking is able to close the interpretability gap between CNNs and transformers, and even make CNNs more interpretable in many cases.

1. Introduction

While deep learning methods have become extremely successful in solving many computer vision tasks, they are generally opaque, and they do not admit easy debugging of errors. Many novel interpretability methods have been developed in recent years which attempt to analyze the reasons behind a model's predictions. In particular, it is natural to analyze the dependence of the model prediction on its input by perturbing parts of its input and observing corresponding changes in the output [14, 18, 29]. Common perturbations include adding Gaussian noise, Gaussian blurring, replacing with a baseline color, etc. However, many of these perturbation methods come with certain downsides. *Partial perturbations*, like Gaussian noise or blurring, attempt to slightly corrupt parts of the image , while still preserving much of the information present in those parts. While this has the advantage of not changing the input distribution drastically, we can only measure the local sensitivity of the model - if the model were to be robust to these perturbations, it would be locally insensitive to perturbations on certain parts of the image but it might still rely heavily on them for its prediction [21, 25]. *Full perturbation* methods remove the parts completely, and replace it with a baseline color like black or grey. In discrete domains like natural language, this is often the most popular method, as it is easy to remove words from the input [15]. In vision, however, this creates a large shift in input distribution, leading the model to perform poorly on such inputs. In particular, it has been shown [10, 23, 24] that CNNs can be sensitive to the mask patterns and the baseline color, focusing more on the mask than the unmasked input.

In recent work [7, 17, 20], it has been observed that vision transformers [5] are highly robust to many kinds of large magnitude input perturbations like occlusions and domain shifts, maintaining upto 60% accuracy on ImageNet even if 80% of the input is randomly blacked out. Jain et al [10] argue that this property can make interpretability methods based on full perturbation especially effective for transformers. They further propose to simply drop tokens corresponding to masked out input parts instead of blacking out or greying out image portions, just like dropping BPE tokens in a transformer-based language model. This would make the transformer model completely insensitive to choice of baseline color and the masking patterns.

Motivated by the same intuition, we devise a new masking technique for CNNs which mitigates the drawbacks of full perturbation to a large extent, which we call **layer masking**. Layer masking (as depicted in Fig. 1) works by running the CNN only on the unmasked portion of the image, thus avoiding any large distribution shift. This is done by carefully masking and padding the input of each layer to make the model focus only on the unmasked input regions. Using this technique, we are able to randomly remove upto 50 % of the input to a ResNet-50 (in the form of 16×16 sized patches) while maintaining the top-1 accuracy on ImageNet over 70%, which is comparable to the robustness of

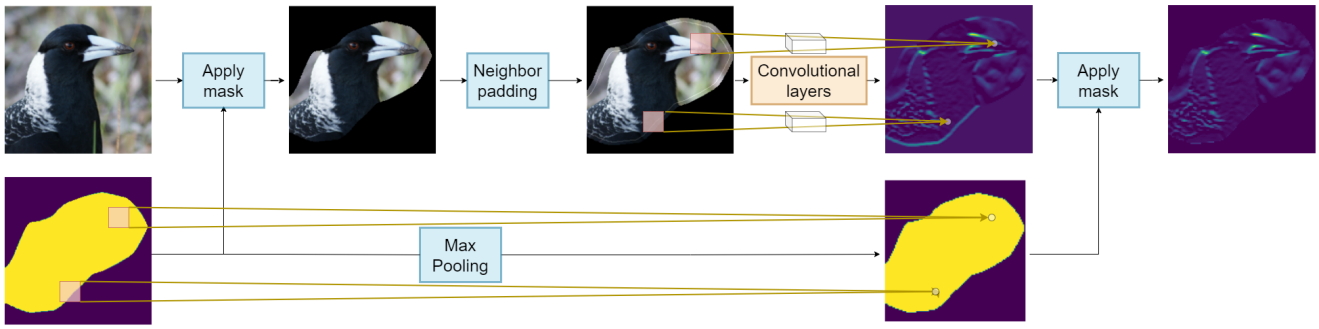

Figure 1. An outline of layer masking, our proposed method, for a convolutional layer. The image is first masked and then padded using neighbor padding. The convolutional layer then acts on the padded image, and a maxpool of the same kernel size and stride acts on the mask. These are then propagated forward through the CNN. The mask boundary is highlighted in the padded image for illustrative purposes.

vision transformers to patch occlusion. In addition, layer masking operates at the pixel level and is thus much more flexible than token dropping for vision transformers which only acts on a patch level. We also find that LIME [18] scores obtained using our masking method are more aligned with the class object around 80% of the time as compared to simply blacking or greying out the masked portion.

2. Related Work

Many interpretability methods designed for computer vision [6, 14, 18, 29] analyze model predictions by implicitly relying on the ability to remove features from the input. Frequently, the removed input features are either masked out and replaced by a "neutral" baseline color like black or grey, or perturbed partially by blurring or adding Gaussian noise. It has been shown in [23, 24] that many of these baseline colors are not really neutral, and interpretability methods which rely on this notion can often be quite sensitive to choice of baselines. Secondly, the models can also be sensitive to the shape of the masking patterns, for example, when randomly masking out 16×16 sized image patches in, ResNets are more likely to predict that the image is a maze or crossword [10]. While partial perturbation methods like adding Gaussian noise may not have similar issues, they can be misleading when the model is insensitive to such perturbations and its output doesn't change significantly [21, 25]. To solve the problem of distribution shift created due to the masking patterns, it was proposed in [9] to retrain the model with the input perturbed according to the patterns utilized in the interpretability methods. While this indeed solves the problem, there are two downsides: (1) the model that is interpreted is not the original model and only a surrogate, and thus may not be very useful for interpretability, and (2) retraining the model with the masking pattern added is expensive. We also have methods like inpainting the masked region using a deep generative model [3]. While this can produce natural images and removes all the original information, it requires training a generative model which can lead to information leakage - for example, if a dog's snout was masked out using this method, the generative model may regenerate the dog's snout again if that is the most likely completion.

There have also been a cluster of papers [7, 10, 17, 20] showing that vision transformers can be very robust (especially compared to CNNs) to many kinds of perturbations including occlusions, patch permutation, adversarial perturbations, distribution shift, etc. In connection to this, it was proposed in [10] that interpretability methods on vision transformers are significantly less sensitive to masking patterns and baseline colors, and also, it is possible to simply drop the necessary patch tokens rather than substituting with a baseline color. In line with this work, we attempt to provide a similar masking method for CNNs which performs as well or better than token dropping for ViTs.

In patch attacks [2], the adversary is allowed full control over a small contiguous portion of the image. These attacks are of special interest because they are physically realizable [11, 27] and can be a realistic way to attack neural networks. Defenses against patch attacks [12, 13, 19, 28] use image masking to try and mask out the portion of the image in control of the adversary. In some of these works, the model is retrained on the images with random features masked out to mitigate any distribution shift, as in [9], while in others there is no retraining. We believe that our work can be complementary to this line of work as it can improve the accuracy of the robust classifier without needing to retrain the model.

3. Proposed Method: Layer Masking

3.1. Motivation

We design a novel feature masking technique for convolutional neural nets (CNNs) which we call *layer masking*.

We are given a model, an input image, and a mask for the input image, and we aim to compute the model output such that (1) it doesn't depend on the masked out portion of the input and (2) it only depends on the unmasked portion of the input, and not the mask pattern itself.

Modern CNNs primarily consist of convolutional layers, along with other layers like batch normalization, max pooling, average pooling, ReLU activations, etc. We can categorize these layers according to the size of their receptive fields. Layers with small receptive fields include convolutional layers, max-pooling and average pooling layers with kernel size much smaller than the size of the image. Fully connected layers, on the other hand, have a large receptive fields as each output depends on all the inputs. Layers with a small receptive field are in general more interpretable because they have fewer parameters and are implicitly hierarchical: for example, a stack of convolutional layers with a small kernel size processes local information first and then progressively expands its receptive field to encompass the whole image. We exploit this structure by devising an algorithm which carefully masks the input and output at *each layer with small receptive field* such that information loss and artifacts created by the masking procedure at each step is minimal. We propagate both the input and the mask at each layer so as to simulate running a CNN on an irregularly shaped input corresponding to the unmasked input features, rather than substituting the masked inputs with a baseline color. We are careful, however, to **not** propagate forward any information in the masked out input regions.

Let the input to a convolutional layer with small receptive field be $\boldsymbol{x} \in \mathbb{R}^{c \times n \times n}$ with output $\boldsymbol{y} \in \mathbb{R}^{c' \times n' \times n'}$ and binary input mask $\boldsymbol{m} \in \{0,1\}^{n \times n}$ ($\boldsymbol{m}[u,v] = 1$ implies that cell (u,v) is unmasked, else it is masked out). Each element of the output of this layer with kernel size $k \times k$ depends on at most k^2 input values. These input values may either be all masked, all unmasked or partially masked and unmasked (when the convolution is over the mask edge), depending on the values of $\boldsymbol{m}$ over the receptive field.

It is clear that our masking procedure should propagate forward the outputs which only depend on the unmasked input, and discard those outputs which depend only on the masked portion. However, it is not immediately obvious how to handle the outputs from the convolutions over the mask edge. The challenge here is that edge convolutions contain valuable information about the edges, and if we discard them at each layer, the unmasked portion of the image can quickly vanish to zero. Thus, we choose to propagate forward the edge convolutions. However, there is the danger of them distorting the natural distribution of the layer activations, as the output unavoidably depends on the masked out region which is filled with zeros. For example, in the third figure (bottom row) of Fig. 2, we see a slice of the activations obtained after applying the 1st residual block of ResNet-50 on the image with the central square region masked out at every layer, but including all the edge convolutions in the output. We see that the convolutions at the top edge of the mask result in a brighter top edge which indicates high activations. This is undesirable since this is an artifact created due to the masking method. We hypothesize that this is because the abrupt transition between the unmasked input and zeros trigger the filters sensitive to edges, thus creating a large activation.

To mitigate this issue, rather than just fill the masked out portion with zeros, we pad the unmasked portion using a variant of replication padding we call **neighbor padding**. Specifically, we iteratively assign the masked input cells adjacent to the mask edge with the average value of its immediate non-zero neighbors. This process is continued till the width of the padding is at least k, the kernel size of the layer. In Fig. 3, we see that after the cells near the edge are progressively filled using the values of its neighbors, the resultant image looks very natural and there is no sharp discontinuity near the edge. We find experimentally that this works much better than padding with zeros (see Tab. 3).

Algorithm 1 Neighbor padding algorithm

Input: Input to be padded $\boldsymbol{x}$, Mask $\boldsymbol{m}$, padding width k
Output: Padded input $\boldsymbol{x}'$
Initialize $\boldsymbol{x}' \leftarrow \boldsymbol{x} \odot \boldsymbol{m}$, $\quad \epsilon \leftarrow 10^{-8}$
Initialize $\boldsymbol{f} \leftarrow \mathbf{1}_{3\times 3}$, a 3×3 filter filled with ones
for $i = 1$ **to** k **do**
  $\boldsymbol{n} \leftarrow \boldsymbol{x}' * \boldsymbol{f}$ // Numerator of the neighbor average
  $\boldsymbol{d} \leftarrow \boldsymbol{m} * \boldsymbol{f}$ // Denominator of the neighbor average
  $\boldsymbol{e} \leftarrow (1 - \boldsymbol{m}) \odot \boldsymbol{n}/(\boldsymbol{d} + \epsilon)$ // Fill masked inputs
  $\boldsymbol{x}' \leftarrow \boldsymbol{x}' + \boldsymbol{e}$
  $\boldsymbol{m} \leftarrow \min(\mathbf{1}, \boldsymbol{m} + \boldsymbol{d})$ // Update masks
end for

We also have to propagate the masks forward, such that for the output of any layer, the propagated mask at that layer is of the same shape as the output and indicates which output values need to be masked out by the following layers. Since edge convolutions are not discarded at any step, the propagated mask must contain 1 for all output cells which depends on the unmasked portion of the input, and 0 everywhere else.

3.2. Formal Description

We now describe our method more formally. Suppose we are given a CNN f which is structured like a directed acyclic graph. Each node of the DAG represents a layer or operation which acts on the outputs of the nodes with which it has an incoming edge. We replace each layer with its masking version (subscripted with m) which acts on an input-mask pair. Let g_k be a layer with receptive field of size k. Then, we define its masking version:

$$g_{k,m}(\boldsymbol{x}, \boldsymbol{m}) = (g_k(\text{Pad}_k(\boldsymbol{x}, \boldsymbol{m})), \text{MaxPool}_k(\boldsymbol{m})))$$

In this equation, g_k could be any convolutional or pooling layer with kernel size k and some stride s. MaxPool_k is a max pooling layer with the same kernel size and stride as g_k. $\text{Pad}_k(\boldsymbol{x}, \boldsymbol{m})$ is a function which neighbor pads $\boldsymbol{x} \odot \boldsymbol{m}$ with padding width k (described in Algorithm 1). Here, $\odot$ is the Hadamard product (with suitable broadcasting), and $*$ is convolution with zero padding. The max pool layer ensures that the output masks contains a 1 for all convolutions where even a single input was unmasked.

Layers which act independently on each element (like ReLU and BatchNorm) can be considered to be a special case of the above with $k = 1$. In this case, the above equation is greatly simplified and becomes:

$$g_m(\boldsymbol{x}, \boldsymbol{m}) = (g(\boldsymbol{x} \odot \boldsymbol{m}), \boldsymbol{m})$$

In models like ResNet which use residual connections, two sets of activations can be added together. We can add two input - mask pairs as:

$$(\boldsymbol{x}_1, \boldsymbol{m}_1) + (\boldsymbol{x}_2, \boldsymbol{m}_2) = ((\boldsymbol{x}_1 + \boldsymbol{x}_2) \odot (\boldsymbol{m}_1 \odot \boldsymbol{m}_2), \boldsymbol{m}_1 \odot \boldsymbol{m}_2)$$

Note that we lose some information here by taking the Hadamard product of the masks, but this is negligible in practice. For fully connected layers, there are hardly any output values which depend on only the masked or unmasked portion of the image. Thus, we allow the fully connected layer to operate normally on its input, replacing the masked portions of the input with a zero baseline value. If h is a fully connected layer, then we define its masking version:

$$h_m(\boldsymbol{x}, \boldsymbol{m}) = h(\boldsymbol{x} \odot \boldsymbol{m})$$

Any layers after a fully connected layer act on the input as normal. We can now create a new model f_m which has the same DAG structure of the original model f, except each layer g^i or h^i has been replaced with the corresponding masking version g^i_m or h^i_m. f_m acts on an image - mask pair and produces an output which depends only on the unmasked portion of the image.

4. Experiments

We perform our experiments on CNNs (ResNet-50 [8]) and vision transformers (ViT-B/16 [5]) pretrained on ImageNet-1000 [4]. The datasets we use are thus also subsets of ImageNet. We analyze and compare the following input masking methods: (1) **Layer masking**, as described in Sec. 3 (only for CNNs), (2) **Token dropping**, as described in [10] (only for ViTs), (3) **Grey-out**: Replace the masked out input with a grey baseline color equal to the ImageNet mean and (4) **Black-out**: Replace the masked out input with a black baseline color.

We also use the following segmentation algorithms to extract the segments from the image (see Fig. 4 for a pictorial representation of these) (1) **Square patches**: Segment the 224×224 image into smaller square patches (typically 16×16), (2) **SLIC superpixels** [1]: Segment the image by clustering pixels based on similarity in the color space and local proximity, and (3) **Quickshift** [26]: Segment the image by first computing a kernel density estimate of the pixel distribution, and then connect each pixel to its nearest neighbor with higher density. We tune hyperparameters for these algorithms such that they divide the image into approximately the same number of segments.

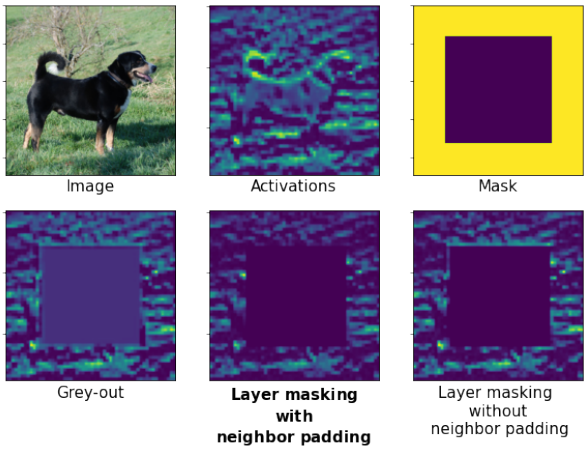

Figure 2. **Top row:** A dog image, sample activations after the first residual block, and mask to be applied to the image. **Bottom row:** The same activations when using grey-out masking, layer masking with neighbor padding (our method), and layer masking without neighbor padding (using zero padding). Neighbor padding helps in eliminating undesirable edge artifacts encountered in zero padding and greying out. Layer masking completely zeros out the masked out region unlike greying out which has non-zero values after a few layers

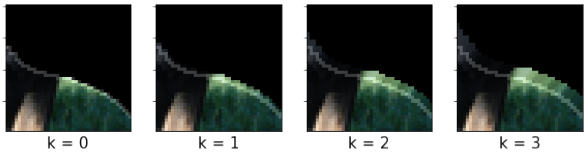

Figure 3. A visual depiction of neighbor padding on a part of the image as k increases. The grey line is the mask edge (added in for illustrative purposes), the cells near the edge are filled progressively with the average of their neighbors' values

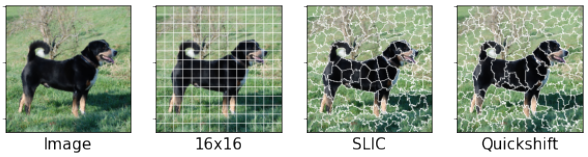

Figure 4. Segmenting (a) an image of a dog using (b) 16×16 patches, (c) SLIC and (d) Quickshift

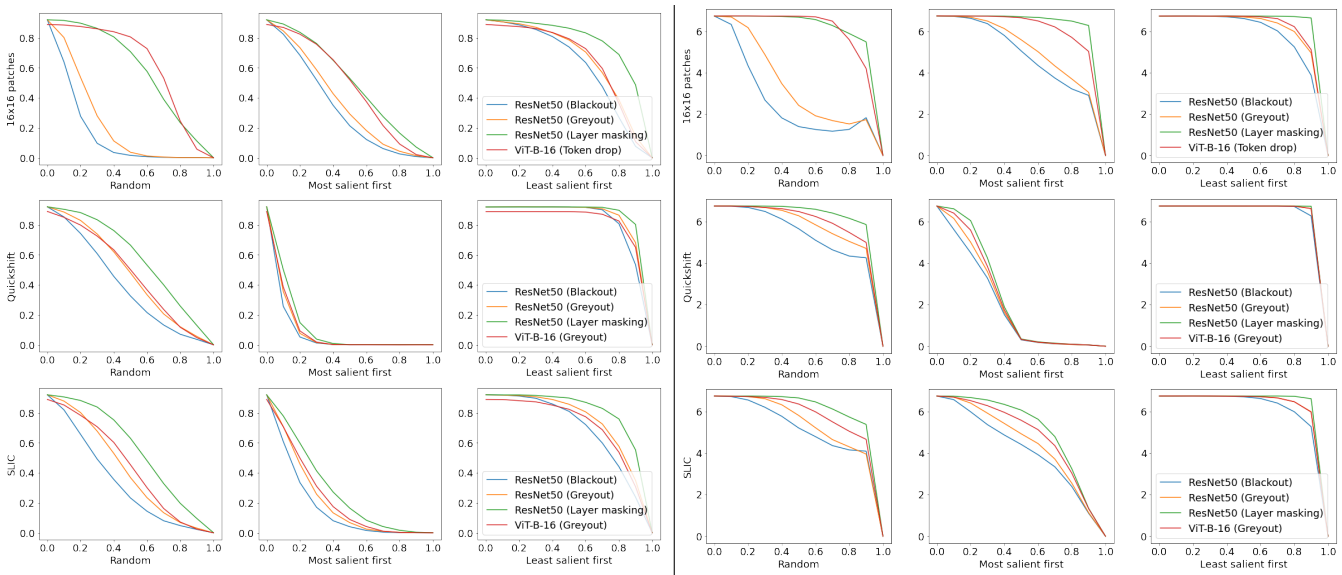

(a) Accuracy (b) Class entropy

Figure 5. Changes in model accuracy and class entropy vs fraction of 16×16 patches(1st row), Quickshift segments (2nd row) and SLIC segments(3rd row) masked out in (1st column) random order, (2nd column) most salient first, and (3rd column) least salient first. ResNets with layer masking are clearly less sensitive to segment removal, especially removal of 16×16 patches. They are also unbiased by the mask shape, unlike ResNets with greyout or blackout masking which predict classes like maze and crossword when 16×16 patches are blacked out or greyed out. ResNets with layer masking match or exceed robustness of ViTs to patch occlusions. *Note: Quickshift produces many very small segments which are not very salient, thus when removing the half of the most salient quickshift segments, most of the image is removed, which is why accuracy and class entropy falls more quickly for quickshift.*

4.1. Segment ablation experiments

To quantify the effect of feature masking methods on the model predictions, we study the behavior of the model when varying parts of the input are masked out. We first segment the image using a segmentation algorithm. Then, we analyze how the model output changes when more and more segments are masked out using the above masking techniques. We characterize the model behavior using 4 metrics: accuracy, class entropy (defined as entropy of $p_f(y) = \mathbb{E}_{\boldsymbol{x} \in D}[1[f(\boldsymbol{x}) = y]]$), WordNet similarity [16] between predictions and true labels, and fraction of unchanged predictions. The WordNet similarity measures how similar the model predictions are to the true labels on a scale from 0 to 1 in place of a binary hit / miss. The fraction of unchanged predictions is a measure of the number of predictions changed by masking out parts of the input image.

In line with previous work [10, 17], we mask out these segments in three ways: (1) Randomly, (2) Most salient first, (3) Least salient first. We then evaluate the metrics listed above, and plot them as a function of the fraction of segments masked out. The accuracy and class entropy plots are shown in Fig. 5, while the rest can be found in the appendix. For the sake of clarity, we report only the best performing baseline for vision transformers, which is token dropping [10] when the segments are 16×16 patches, but greyout masking for other segmentation methods.

Computing the saliency scores: We select 5000 random images and saliency maps from Salient ImageNet [22] for our experiment. Each saliency map $m \in \mathbb{R}^{d \times d}$ is a pixel level saliency attribution array where $0 \leq m[i,j] \leq 1$ denotes the importance of the (i,j)th pixel to predicting the ImageNet class - the higher the value, the more important the pixel is. Each image is first segmented using a given segmentation algorithm. We then compute saliency scores for each segment by summing up the saliency values for all pixels in that segment.

We expect that an ideal masking technique should affect the model output minimally, under the constraint that the model does not rely on information in the parts of the image which are masked out. It should also not be biased by the masking pattern to predict certain classes more than others. We measure the model prediction quality using accuracy, WordNet similarity and change in model predictions, and the extent of masking bias using class entropy - the higher the class entropy, the less biased the masking.

We observe that, consistent with [10, 17], vision transformers are more robust to image occlusion as compared to ResNets when greying out or blacking out the image. Specifically, we find that transformers are much more robust to perturbations which are aligned with the patch bound-

aries of the vision transformer (like occluding 16×16 sized patches for ViT-B/16), but are more sensitive to occlusions of irregularly shaped regions, as found in SLIC or quickshift segments. However, if layer masking is used, ResNets can be much more robust to such occlusions irrespective of its shape, exceeding robustness of transformers in many cases. The class entropy plots show that layer masking does not bias the model towards predicting certain classes. Greying or blacking out segments however, makes the model predict certain classes more than others - for example, greying out 16×16 patches causes the model to predict ImageNet classes like 'maze' or 'crossword' which resemble the masking pattern [10]. We thus find that layer masking is superior to greying out or blacking out across all cases.

4.2. Impact on interpretability methods

Many interpretability methods [14, 18, 29] rely on the notion of a "neutral" masking technique in order to evaluate the influence of different parts of the image on the model prediction. This is generally not true and the masking technique can have a significant impact on the importance scores given by the interpretability method. We investigate the effect of masking methods on interpretability in this section using the example of LIME.

4.2.1 Visual inspection

We first visually illustrate the impact of masking technique on LIME using a couple of examples in Fig. 6. For the LIME explanations, the top 10 segments with the highest magnitude LIME score are highlighted. Red segments detract from the prediction, and a green segments contribute to the prediction. In the image of a cat and a mouse, the model misclassifies the black cat as an 'American black bear' or a 'groenendael' (a black dog breed). But LIME assigns a highly negative score (in red) to certain regions of the black cat for the 'groenendael' and 'black bear' prediction when masking using blacking or greying out, which seems incorrect. Similarly, in the image of a cat and a dog, LIME with greyout or blackout masking assigns parts of the cat high positive scores (in green) and parts of the dog negative scores (in red) in the explanation of the prediction of Bernese mountain dog, and vice versa for the explanation of the tabby prediction. The third column containing the LIME explanations obtained using layer masking is much more aligned with human intuition.

4.2.2 Quantitative evaluation

To get a better sense of the effect of masking techniques on LIME, we perform a quantitative evaluation. For each prediction, LIME assigns an importance score s_i to each image segment i, where a positive score of high magnitude means that the segment contributes highly to the prediction, but a negative score means that the segment detracts from the prediction. To evaluate explanations quantitatively in the absence of a reliable ground truth, we use the images and segmentation masks from Pixel ImageNet [30] as a substitute for the "correct" explanation. Given a segmentation mask $\boldsymbol{m} \in [0,1]^{d \times d}$ for an image of dimension d, we derive the "ground truth" $\boldsymbol{g}$ for the explanation such that $\boldsymbol{g}_i = \sum_{(u,v) \in \text{patch } i} (\boldsymbol{m}[u,v] - m_{avg})$ where m_{avg} is the mean of the segmentation mask. We can then measure how aligned the explanations are with the ground truth by computing the *alignment score*, which is the cosine similarity between g_i and s_i, or $\cos(\boldsymbol{g}, \boldsymbol{s}) = \frac{\sum_i g_i s_i}{\sqrt{(\sum_i g_i^2)(\sum_i s_i^2)}}$. The alignment score will be 1 if the LIME explanation $\boldsymbol{s}$ is perfectly aligned with $\boldsymbol{g}$, and -1 if it is completely misaligned.

	Blackout	Greyout	**Layer masking**
ResNet-50			
Quickshift	0.1153	0.2211	**0.3042**
SLIC	0.1235	0.2186	**0.3120**
16 x 16 patches	0.0119	0.0675	**0.2253**
ViT/B-16			Token dropping
Quickshift	0.1693	0.2417	0.0444
SLIC	0.1748	0.2446	0.0539
16 x 16 patches	0.1633	0.1678	0.1430

Table 1. Mean alignment scores for LIME computed over 500 randomly sampled images from Pixel ImageNet [30]

	Blackout	Greyout	**Layer masking**
ResNet-50			
Quickshift	0.106	0.228	**0.666**
SLIC	0.078	0.206	**0.716**
16 x 16 patches	0.040	0.146	**0.814**
ViT/B-16			Token dropping
Quickshift	0.292	0.594	0.114
SLIC	0.270	0.614	0.116
16 x 16 patches	0.366	0.396	0.238

Table 2. Mean win rate for LIME computed over 500 randomly sampled images from Pixel ImageNet

We measure alignment scores for different masking methods for ResNet-50 and ViT over 500 images from Pixel ImageNet and report them in Tab. 1. In these 500 images, the correct class is within the top 3 predictions of the model. In general, ViTs have better scores for greyout and blackout than the corresponding scores for ResNet-50, especially for 16×16 sized patches. We find that token dropping in vision transformers is not the best solution - although it performs somewhat well if the segments are 16×16 patches, it fails when the segments are irregularly shaped. This is because token dropping operates at the patch level and has to discard more patches and more information than greying out or blacking out in order for it to not rely on any masked

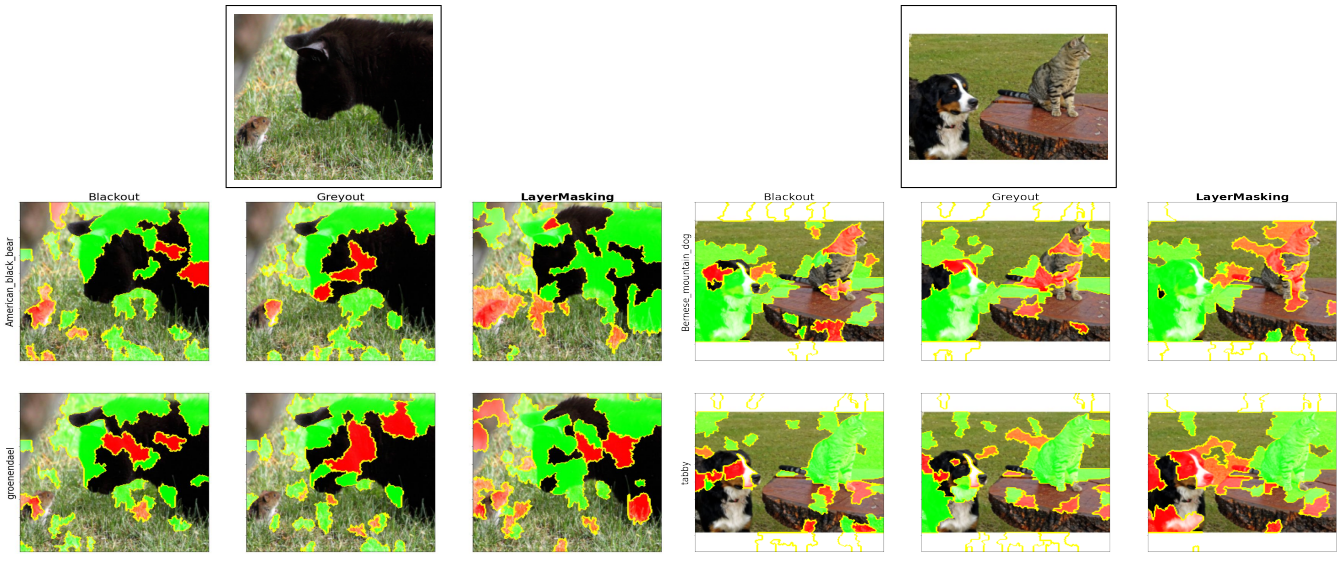

(a) A cat and a mouse

(b) A dog and a cat

Figure 6. Visualization of LIME scores for the top two predictions of ResNet-50 on two sample images. Columns correspond to the masking techniques (blacking out, greying out, and layer masking), rows are the top 2 predictions. For (a), the top two predictions are American black bear and Groenendael. For (b), they are Bernese mountain dog and tabby cat. Green regions contribute to the prediction, red regions detract from the prediction.

out information. However, layer masking does not suffer the same problems. We find that layer masking is much superior to blacking or greying out the input across different segmentation algorithms. In fact, the alignment scores for ResNet-50 with layer masking are better than the best numbers for ViTs, which suggests that ResNets can be more interpretable than ViTs when combined with layer masking.

However, note that the alignment scores can vary quite a lot over many images. For example, there might be some images on which LIME works well, and others where it fails, leading to a large variation in alignment scores. Therefore, it might be misleading to just report the average alignment score. We also calculate the *win rate* for each masking technique, which is the fraction of images for which that particular masking technique had the best alignment score compared to the other techniques in Tab. 2. The win rates sum up to 1 in each row. We find that trends are broadly similar to those in Tab. 1. Layer masking wins over regular black or grey masking 65% to 80% of the time.

4.3. Ablation study

To further investigate the effect of layer masking and neighbor padding on model behavior, we construct 3 variants of layer masking: (a) With zero padding instead of neighbor padding (b) Masking and padding only the first two residual blocks, (c) Masking and padding only the first convolutional layer, ReLU and BatchNorm layer

Using a similar setup as in Sec. 4.1, we we compute the area under curve (AUC) for each plot of metric vs fraction of segments dropped. The AUC values are averaged over different segmentation algorithms (SLIC, quickshift, etc) and masking orders (random, salient first, etc)(refer Tab. 3).

	Accuracy	Class Entropy	Wordnet Similarity	Unchanged Predictions
Blackout	0.3881	4.6473	0.6930	0.4094
Greyout	0.4398	4.9408	0.7167	0.4636
Layer masking:				
On all layers	**0.5604**	**5.6021**	**0.7881**	**0.5907**
On 1st and 2nd residual blocks	0.5103	5.0962	0.7616	0.5391
Zero padding	0.4502	5.0388	0.7262	0.4747

Table 3. Average AUC for different variants of layer masking alongside the black out and grey out baselines (model: ResNet-50). Higher the better

We find that both neighbor padding and masking all layers are important to the masking technique. Layer masking with zero padding is still better than blackout or greyout, but much worse than with neighbor padding. Layer masking only the first two residual blocks is also inferior to masking through all layers, but we find that there are diminishing returns, as we are able to obtain much of the improvement by masking only half of the layers.

4.4. Other interesting properties of layer masking

In this section, we identify some more properties of layer masking that are important for model interpretability.

Linearity in masking: Consider a model equipped with

a masking technique f_m which acts on an input - mask pair $(\boldsymbol{x}, \boldsymbol{m})$ and returns an output $\boldsymbol{y}$ which depends only on the unmasked parts of the input. Then, we say that the model f_m is linear in masking if $f_m(\boldsymbol{x}, \boldsymbol{m}_1 + \boldsymbol{m}_2) = f_m(\boldsymbol{x}, \boldsymbol{m}_1) + f_m(\boldsymbol{x}, \boldsymbol{m}_2)$ for any two binary masks $\boldsymbol{m}_1, \boldsymbol{m}_2$ such that $\boldsymbol{m}_1 \cdot \boldsymbol{m}_2 = 0$. This property is useful for interpretability methods like LIME which train a linear model on $(\boldsymbol{m}, \boldsymbol{y})$ pairs and use its weights to explain the model prediction. Modern vision models like CNNs and Vision Transformers are non-linear and include cross-interactions between features in $\boldsymbol{m}_1$ and $\boldsymbol{m}_2$. Thus, it is not possible to design a perfectly linear masking technique for these architectures, which means that only approximate linearity is possible. However, we can attempt to design more linear masking methods for each model architecture, and thus obtain more interpretable masking techniques.

We measure linearity by sampling random images from ImageNet and dividing it into N smaller square patches. We can then compute the cosine similarity between $f(\boldsymbol{x})$ and $\sum_{i=1}^{N} f_m(\boldsymbol{x}, \boldsymbol{m}_i)$ where $\boldsymbol{m}_i$ corresponds to patch i (Tab. 4). We find that layer masking is much more linear as compared to greying out or blacking out pixels, and in general, ResNet masking methods are more linear than corresponding methods for ViTs. Because the attention heads in ViTs introduce a lot of cross terms right from the beginning, including cross terms between distant patches, linearity in vision transformer masking is much lower than CNN masking.

We also find that in layer masking, $\mathbb{E}_{\boldsymbol{x}} \|f_m(\boldsymbol{x}, \boldsymbol{m})\|$ scales linearly with $|\boldsymbol{m}|$. We test this by measuring the magnitude of $f_m(\boldsymbol{x}, \boldsymbol{m})$ with $\boldsymbol{m}$ as a mask for square patches of side length n, so that $\|\boldsymbol{m}\| \propto n^2$. We observe in Fig. 8 that layer masking closely tracks the n^2 curve, which implies that $\mathbb{E}_{\boldsymbol{x}} \|f_m(\boldsymbol{x}, \boldsymbol{m})\|$ scales almost linearly with $\|\boldsymbol{m}\|$ for layer masking. However, the magnitude for ViT features remain approximately constant.

Avoidance of output collapse: As the fraction of masked input approaches 1, it is desirable to avoid the model output collapsing to the same vector and thus not being sensitive enough to the unmasked features. To test for this, we take two random images $\boldsymbol{x}_1$ and $\boldsymbol{x}_2$ of size 224×224 and compute the cosine similarity between their model features, $c = \cos(f(\boldsymbol{x}_1), f(\boldsymbol{x}_2))$. Then, these images are resized to a smaller size n, and padded with zeros to recover the original size . We now have images $\boldsymbol{x}_{1,n}$ and $\boldsymbol{x}_{2,n}$ of size 224×224 and a mask of the same shape $\boldsymbol{m}_n$ which is 1 for a region of size $n \times n$ and 0 elsewhere. We then measure the cosine similarity between $\boldsymbol{x}_{1,n}$ and $\boldsymbol{x}_{2,n}$ as $c_n = \cos(f_m(\boldsymbol{x}_{1,n}, \boldsymbol{m}_n), f_m(\boldsymbol{x}_{2,n}, \boldsymbol{m}_n))$ and plot $\mathbb{E}_{\boldsymbol{x}_1, \boldsymbol{x}_2}[c_n - c]$ as function of n in Fig. 7. We clearly see that as the image size is decreased, the cosine similarity changes much more for greyout or blackout as compared to layer masking for ResNet-50 or token dropping for ViTs.

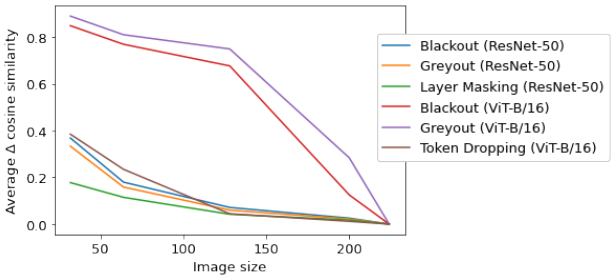

Figure 7. Average difference in cosine similarity vs image size. Since model features of ViTs can be negative unlike ResNet-50, cosine similarity can vary from -1 to 1

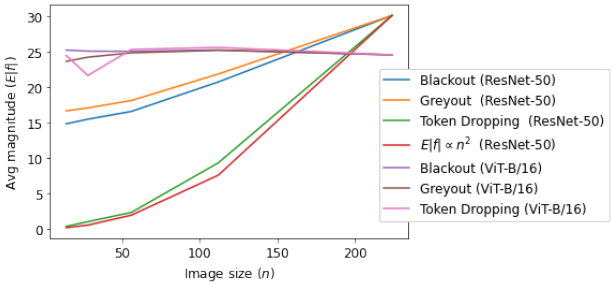

Figure 8. Mean magnitude of output feature vectors vs image size

	ResNet-50			ViT-B/16		
Patch size	Blackout	Greyout	**Layer masking**	Blackout	Greyout	Token dropping
112	0.7975	0.8284	**0.9485**	0.6707	0.7063	0.7043
56	0.5124	0.5842	**0.8310**	0.2202	0.2506	0.1929
32	0.4282	0.4878	**0.7094**	0.1377	0.1365	0.1426
16	0.3848	0.4371	**0.6490**	0.0912	0.0876	0.0877

Table 4. Average cosine similarity between image features and their linear approximation

5. Conclusion

In this paper, we have presented a new masking technique such that the model output is both (a) perfectly insensitive to the masked out portion of the input and (b) only focused on the unmasked input and not the masking pattern. We find that layer masking can make CNNs like ResNets very robust to input removal without retraining - comparable to vision transformers - especially when the masking patterns can get confused with output classes like patch occlusions. We further find that LIME scores obtained using layer masking are better than LIME scores with blacking or greying out for up to 80% of the images in Pixel ImageNet. We propose that this technique can be of great use in interpretability techniques like LIME which rely on the ability to remove features from the input without any major distribution shift.

References

[1] Radhakrishna Achanta, Appu Shaji, Kevin Smith, Aurelien Lucchi, Pascal Fua, and Sabine Süsstrunk. Slic superpixels compared to state-of-the-art superpixel methods. *IEEE Transactions on Pattern Analysis and Machine Intelligence*, 34(11):2274–2282, 2012. 4

[2] Tom B Brown, Dandelion Mané, Aurko Roy, Martín Abadi, and Justin Gilmer. Adversarial patch. *arXiv preprint arXiv:1712.09665*, 2017. 2

[3] Chun-Hao Chang, Elliot Creager, Anna Goldenberg, and David Duvenaud. Explaining image classifiers by counterfactual generation. In *International Conference on Learning Representations*, 2019. 2

[4] Jia Deng, Wei Dong, Richard Socher, Li-Jia Li, Kai Li, and Li Fei-Fei. Imagenet: A large-scale hierarchical image database. In *2009 IEEE conference on computer vision and pattern recognition*, pages 248–255. Ieee, 2009. 4

[5] Alexey Dosovitskiy, Lucas Beyer, Alexander Kolesnikov, Dirk Weissenborn, Xiaohua Zhai, Thomas Unterthiner, Mostafa Dehghani, Matthias Minderer, Georg Heigold, Sylvain Gelly, Jakob Uszkoreit, and Neil Houlsby. An image is worth 16x16 words: Transformers for image recognition at scale. In *International Conference on Learning Representations*, 2021. 1, 4

[6] Ruth C Fong and Andrea Vedaldi. Interpretable explanations of black boxes by meaningful perturbation. In *Proceedings of the IEEE international conference on computer vision*, pages 3429–3437, 2017. 2

[7] Jindong Gu, Volker Tresp, and Yao Qin. Are vision transformers robust to patch perturbations? In Shai Avidan, Gabriel Brostow, Moustapha Cissé, Giovanni Maria Farinella, and Tal Hassner, editors, *Computer Vision – ECCV 2022*, pages 404–421, Cham, 2022. Springer Nature Switzerland. 1, 2

[8] Kaiming He, Xiangyu Zhang, Shaoqing Ren, and Jian Sun. Deep residual learning for image recognition. *CoRR*, abs/1512.03385, 2015. 4

[9] Sara Hooker, Dumitru Erhan, Pieter-Jan Kindermans, and Been Kim. A benchmark for interpretability methods in deep neural networks. In H. Wallach, H. Larochelle, A. Beygelzimer, F. d'Alché-Buc, E. Fox, and R. Garnett, editors, *Advances in Neural Information Processing Systems*, volume 32. Curran Associates, Inc., 2019. 2

[10] Saachi Jain, Hadi Salman, Eric Wong, Pengchuan Zhang, Vibhav Vineet, Sai Vemprala, and Aleksander Madry. Missingness bias in model debugging. In *International Conference on Learning Representations*, 2022. 1, 2, 4, 5, 6

[11] Mark Lee and Zico Kolter. On physical adversarial patches for object detection. *arXiv preprint arXiv:1906.11897*, 2019. 2

[12] Alexander Levine and Soheil Feizi. (de)randomized smoothing for certifiable defense against patch attacks. In *Proceedings of the 34th International Conference on Neural Information Processing Systems*, NIPS'20, Red Hook, NY, USA, 2020. Curran Associates Inc. 2

[13] Jiang Liu, Alexander Levine, Chun Pong Lau, Rama Chellappa, and Soheil Feizi. Segment and complete: Defending object detectors against adversarial patch attacks with robust patch detection. In *Proceedings of the IEEE/CVF Conference on Computer Vision and Pattern Recognition*, pages 14973–14982, 2022. 2

[14] Scott M Lundberg and Su-In Lee. A unified approach to interpreting model predictions. In I. Guyon, U. V. Luxburg, S. Bengio, H. Wallach, R. Fergus, S. Vishwanathan, and R. Garnett, editors, *Advances in Neural Information Processing Systems 30*, pages 4765–4774. Curran Associates, Inc., 2017. 1, 2, 6

[15] Dina Mardaoui and Damien Garreau. An analysis of lime for text data. In Arindam Banerjee and Kenji Fukumizu, editors, *Proceedings of The 24th International Conference on Artificial Intelligence and Statistics*, volume 130 of *Proceedings of Machine Learning Research*, pages 3493–3501. PMLR, 13–15 Apr 2021. 1

[16] George A. Miller. WordNet: A lexical database for English. In *Human Language Technology: Proceedings of a Workshop held at Plainsboro, New Jersey, March 8-11, 1994*, 1994. 5

[17] Muzammal Naseer, Kanchana Ranasinghe, Salman Khan, Munawar Hayat, Fahad Khan, and Ming-Hsuan Yang. Intriguing properties of vision transformers. In A. Beygelzimer, Y. Dauphin, P. Liang, and J. Wortman Vaughan, editors, *Advances in Neural Information Processing Systems*, 2021. 1, 2, 5

[18] Marco Tulio Ribeiro, Sameer Singh, and Carlos Guestrin. "why should I trust you?": Explaining the predictions of any classifier. In *Proceedings of the 22nd ACM SIGKDD International Conference on Knowledge Discovery and Data Mining, San Francisco, CA, USA, August 13-17, 2016*, pages 1135–1144, 2016. 1, 2, 6

[19] Hadi Salman, Saachi Jain, Eric Wong, and Aleksander Madry. Certified patch robustness via smoothed vision transformers. *CoRR*, abs/2110.07719, 2021. 2

[20] Rulin Shao, Zhouxing Shi, Jinfeng Yi, Pin-Yu Chen, and Cho-Jui Hsieh. On the adversarial robustness of vision transformers, 2021. 1, 2

[21] Avanti Shrikumar, Peyton Greenside, and Anshul Kundaje. Learning important features through propagating activation differences. In Doina Precup and Yee Whye Teh, editors, *Proceedings of the 34th International Conference on Machine Learning*, volume 70 of *Proceedings of Machine Learning Research*, pages 3145–3153. PMLR, 06–11 Aug 2017. 1, 2

[22] Sahil Singla and Soheil Feizi. Salient imagenet: How to discover spurious features in deep learning? In *International Conference on Learning Representations*, 2022. 5

[23] Pascal Sturmfels, Scott Lundberg, and Su-In Lee. Visualizing the impact of feature attribution baselines. *Distill*, 2020. https://distill.pub/2020/attribution-baselines. 1, 2

[24] Mukund Sundararajan and Ankur Taly. A note about: Local explanation methods for deep neural networks lack sensitivity to parameter values. *CoRR*, abs/1806.04205, 2018. 1, 2

[25] Mukund Sundararajan, Ankur Taly, and Qiqi Yan. Axiomatic attribution for deep networks. In *International conference on machine learning*, pages 3319–3328. PMLR, 2017. 1, 2

[26] Andrea Vedaldi and Stefano Soatto. Quick shift and kernel methods for mode seeking. In David Forsyth, Philip Torr, and Andrew Zisserman, editors, *Computer Vision – ECCV 2008*, pages 705–718, Berlin, Heidelberg, 2008. Springer Berlin Heidelberg. 4

[27] Zuxuan Wu, Ser-Nam Lim, Larry S Davis, and Tom Goldstein. Making an invisibility cloak: Real world adversarial attacks on object detectors. In *European Conference on Computer Vision*, pages 1–17. Springer, 2020. 2

[28] Maksym Yatsura, Kaspar Sakmann, N Grace Hua, Matthias Hein, and Jan Hendrik Metzen. Certified defences against adversarial patch attacks on semantic segmentation. *arXiv preprint arXiv:2209.05980*, 2022. 2

[29] Matthew D. Zeiler and Rob Fergus. Visualizing and understanding convolutional networks. *CoRR*, abs/1311.2901, 2013. 1, 2, 6

[30] Shiyin Zhang, Jun Hao Liew, Yunchao Wei, Shikui Wei, and Yao Zhao. Interactive object segmentation with inside-outside guidance. In *Proceedings of the IEEE/CVF Conference on Computer Vision and Pattern Recognition*, pages 12234–12244, 2020. 6